SSRG International Journal of Electrical and Electronics Engineering
ISSN: 2348-8379/ https://doi.org/10.14445/23488379/IJEEE-V13I3P106

Volume 13 Issue 3, 62-80, March 2026

Original Article

Intelligent MPPT for Constant Power Generation using PKOA-RBFNN and Active Clamp Triple Stage Cascade Boost Converter

R. Sreenivasan[1*], R. Ramkumar[2]

[1,2]*Department of Electrical and Electronics Engineering, School of Engineering and Technology, Dhanalakshmi Srinivasan University, Samayapuram, Trichy, Tamil Nadu, India.*

[1*]*Corresponding Author : srini.vasan256@gmail.com*

Received: 07 December 2025 Revised: 08 January 2026 Accepted: 08 February 2026 Published: 31 March 2026

Abstract- *The aim of this research is to enhance the amount of power captured from Photovoltaic (PV) systems by tracking the utmost power in partial shading conditions and uninterruptedly regulating the PV systems to function at the Maximum Power Point (MPP) in climate variations like temperature and irradiance. This study introduces an intelligent MPPT system focused on Constant Power Generation (CPG) that combines an Active Clamp Triple-Stage Cascade (ACTSC) Boost converter with a Radial Basis Function Neural Network (RBFNN) controller with the Pied Kingfisher Optimization Algorithm (PKOA). The ACTSC Boost converter increases voltage gain and reduces losses on the switch, resulting in excellent efficiency. In order to quickly monitor the MPP with fewer steady-state oscillations, the PKOA-optimized RBFNN-MPPT controller constantly modifies its weights and spread parameters. PKOA improves MPPT accuracy under varying irradiance and temperature conditions by ensuring faster convergence, improved flexibility, and global search capabilities. The higher performance of the proposed approach over traditional MPPT algorithms is confirmed by an extensive MATLAB tool, highlighting that the proposed approach has a better efficacy of 94.33%and superior tracking efficiency, thereby offering a reliable and effective solution for contemporary PV applications in grid-connected systems.*

Keywords- *PV System, ACTSC Boost Converter, RBFNN-MPPT Controller, PKOA.*

1. Introduction

1.1. Background

With rising greenhouse gas emissions, rising global temperatures, and frequent extreme weather events that have a substantial impact on both natural ecology and human society, environmental degradation and climate change have become major global challenges in recent years [1]. People need to discover sustainable solutions to these environmental issues immediately in order to diminish dependence on fossil fuels and the rate of climate change. In order to produce clean, non-polluting energy, renewable energy is a thriving, environmentally friendly technology that has recently included more cutting-edge technologies [2-4]. Solar PV power is one of the most widely used RESs due to its many benefits, including being ubiquitous, readily accessible, having no rotating parts, having cheap operating costs, requiring little maintenance, being able to be installed on rooftops, and being environmentally beneficial [5, 6]. To guarantee a consistent energy supply across grids, solar energy production forecasting is essential [7]. However, it faces a number of technical and non-technical difficulties, including low power conversion efficiency, high installation costs, and a strong reliance on atmospheric conditions, which are resolved by a DC/DC converter [8, 9].

2. Literature Survey

The Active Clamp Flyback Converter [10] makes it possible to use more reliable and efficient components by lessening voltage stress on the switch. When compared to a Flyback converter, it has a larger circuit and control complexity. Switching losses, inductor current ripple, and output voltage distortion are minimized by the three-level boost converter [11]. Maintaining voltage balance between the series-connected capacitors is a major operational challenge since imbalances increase voltage stress on the switches and impair overall performance. The enhanced non-isolated quadratic boost converter [12] generates a high gain effect while providing less voltage stress on the capacitors, switch, and diodes. Applications that need safety isolation between input and output are inherently limited by the non-isolated nature. To get the required high output voltage from a low input voltage, a step-up converter [13] is essential for applications such as electric vehicles and RES. Multiple components, such as coupled inductors, switching capacitors,

or voltage multiplier cells, are needed to produce very high gains. This increases the converter's size and expense and lowers dependability. Low voltage, power switch current stress, input current ripple, and a few elements are the benefits of the coupled inductor-based interleaved converter [14]. Its interleaved structure complicates control systems, and its greater turns ratio increases leakage inductance that causes voltage spikes on switches and diodes. The switched inductor/capacitor converter [15] reduces the requirement for large input filters and shields the input source from pulsing currents due to its unremitting input current with less ripple. Because of the internal resistance of the components, the increasing number of switches results in large conduction losses for higher power. Therefore, the ACTSC Boost converter is utilized for raising the PV system's voltage level. The MPPT controller is vital in PV systems owing to the PV array's voltage-current features, which continuously vary with temperature and irradiance conditions. MPPT assures that the PV system functions at its optimal voltage, thereby maximizing power extraction and enhancing efficiency. The conventional MPPT includes the Perturb &Observe (P&O) [16] algorithm, which maintains a better efficiency in uniform conditions and reacts fast to small fluctuations in irradiance. However, it has tracking errors that occurred from misinterpreting environmental changes as power perturbations under quickly changing irradiance. The Genetic Algorithm (GA) [17] uses evolutionary search to explore a large solution space, making it possible to track global MPP reliably even in partial shading.

Nevertheless, the tracking accuracy is impacted by crucial parameter settings, such as crossover and mutation rates. By comparing incremental and instantaneous conductance, Incremental Conductance (INC) enables precise tracking and MPP detection. The implementation cost of INC is increased by the need for numerous sensors and intricate computations [18]. The Artificial Neural Network (ANN) [19] map nonlinear correlations and learn PV features, providing excellent accuracy. To achieve generalization, an ANN needs to be trained extensively offline using a variety of datasets. Insufficient or non-representative training data causes reduced performance. The fuzzy MPPT [20] uses rule-based decision making to handle PV non-linearities; it offers exceptional versatility.

If the rule base is poorly defined or not generalized for different conditions, performance is affected. During training, the Adaptive Neuro Fuzzy Inference System (ANFIS) automatically learns the best rules and membership functions. It provides little oscillation around MPP and quick convergence. Large, excellent training datasets are necessary for ANFIS to function at its best and take a long time and a lot of processing power for the training process [21]. Also, the nonlinear nature of the PV system makes MPPT approaches slow and oscillatory in partial shading conditions. So, the optimization approach is integrated to tune the MPPT parameters and ensure stable tracking of MPP in dynamic environmental conditions. The analysis of existing optimization approaches is revealed in Table 1.

Table 1. Analysis of existing optimization approaches

Approaches	Merits	Drawbacks
Musical chairs algorithm [22]	It offers reduced failure rates and convergence time. At the start of the iteration, there are a lot of search agents, and as the iterations rise, the number of search agents steadily decreases.	The MCA's performance is probably dependent on the particular parameters that are tuned, and poor parameter choices have an impact on its stability or efficiency.
Falcon optimization method [23]	It tracks GMPP more effectively and quickly under a variety of environmental situations.	In addition to increasing the cost and complexity of real-time implementation, it demands greater computing power.
Sooty tern optimization [24]	It has better tracking accuracy, dynamic stability, and convergence speed. It provides accurate and dependable tracking of the global MPP, especially in difficult shading situations.	If its exploration capabilities are inadequate for the search space, it becomes trapped in local optima and struggles to handle difficult partial shading situations.
Dung beetle optimization [25]	Low tracking efficiency, GM oscillation, and power loss are solved by this approach. DBO's tracking efficiency reaches 99.99% in all PSCs, and it has outstanding GMPP tracking capabilities under various weather situations.	It has a slow convergence rate and a propensity to become stuck in local optima, particularly in complex or high-dimensional situations.
Improved coot optimization [26]	It combines a single tuning parameter and a search space skipping technique to increase convergence speed.	To improve system reliability, it is necessary to eliminate the necessity for re-initialization during irradiance changes.
African vulture optimization [27]	In order to obtain the best converter that conforms to the MPP, the African vulture optimization is useful for adjusting the joining weights.	The initial conditions or the vultures' randomly selected starting places have an impact on AVOA's performance.

This paper develops an RBFNN-MPPT controller based on the PKOA in order to overcome these drawbacks. The MPP is effectively and steadily tracked under dynamic environmental conditions due to the inclusion of PKOA, which improves the convergence speed and adaptability of RBFNN-MPPT parameter tuning.

2.1. Research Gap

Attaining consistent and precise maximum power extraction under partial shading and quickly changing environmental circumstances is still a major issue, even with major developments in converter and MPPT approaches. Steady-state oscillations, delayed convergence, and tracking errors during irradiance variations plague traditional MPPT techniques. Real-time adaptability is limited by the large training datasets and significant computing effort required by intelligent techniques. Comparably, a lot of modern optimization methods have problems like high implementation complexity, parameter sensitivity, or premature convergence.

Furthermore, efficiency, voltage stress, ripple, and component count are frequently traded off in current high-gain converters. Research on combining a reliable, fast-converging intelligent optimization-based MPPT that can provide steady power generation with an effective high-gain converter topology is lacking. In order to improve PV system performance in dynamic operating scenarios, an intelligent MPPT framework that is computationally efficient and globally convergent needs to be paired with a high-efficiency boost architecture. This work combines the ACTSC Boost converter with the PKO-RBFNN MPPT controller. It allows for quick, precise, and steady MPPT under dynamic temperature and irradiance variations.

The PKOA-RBFNN adaptively adjusts controller parameters to guarantee global convergence and low steady-state error, in contrast to traditional MPPT techniques that have slow convergence, oscillations, or local optima. The ACTSC Boost maintains high efficiency while lowering voltage stress, switching losses, and DC-link ripple in comparison to earlier high-gain converter designs. In terms of tracking accuracy, response time, and dependability, this integrated methodology performs better than conventional and other bio-inspired MPPT techniques. Additionally, the suggested approach is appropriate for real-time hardware implementation and computationally efficient. As a result, it offers a reliable, high-performing solution for steady power generation in PV systems under variable climatic and partial shade circumstances.

The Main objectives are,

- In order to increase energy conversion efficiency and obtain high voltage gain, this work incorporates an ACTSC Boost converter with efficient power transmission and reduced energy losses.
- To accomplish a quick and accurate Maximum Power Point in dynamic environmental settings, an RBFNN-MPPT controller is developed.
- By optimizing the RBFNN parameters, the incorporation of PKOA improves convergence speed and flexibility.

3. Proposed Methodology

The PV-based system's block diagram for continuous power generation is depicted in Figure 1. The PV system is a primary energy source that is employed in this research due to its clean, renewable, and decentralized power production at reduced expense. Nevertheless, its nonlinear nature produces large variations in output power.

Thus, the ACTSC Boost converter enhances the PV system's voltage with decreased voltage stress and high voltage gain. The cascaded structure is employed to attain high voltage gain, thereby enhancing efficiency and reducing component ratings.

By distributing the voltage boosting process over three stages, the ACTSC Boost converter reduces input current ripple. Then, the active clamp circuit assures reduced switching stress and improved reliability. Subsequently, the RBFNN-MPPT controller integrates the nonlinear mapping ability of RBFNN with the intelligent search capability of PKOA to attain quick and precise maximum power tracking.

The PKOA optimizes the RBFNN-MPPT parameters to improve tracking efficiency and avert convergence to local maxima in partial shading conditions. Consequently, the Pulse Width Modulation (PWM) generator generates PWM pulses based on the duty cycle received from the MPPT controller for better control of the switch in the ACTSC Boost converter. Finally, the obtained DC power is efficiently delivered to the load with stable regulation. Thereby, the system attains better efficiency, stability, and reliability of constant power generation.

4. Modelling of Proposed System

4.1. PV System

A semiconductor device known as a PV cell converts sunlight into electrical energy, as represented in Figure 2. The intensity of the sun, the temperature, and the fundamental characteristics of the cell material all affect a solar cell's efficiency.

Consequently, a PV cell model needs to be developed in order to allow the solar panels to function at their MPP and achieve their photoelectric conversion efficiency by affecting the solar panels' output capacity through the influence of light intensity and external temperature. The expressions of the PV system are,

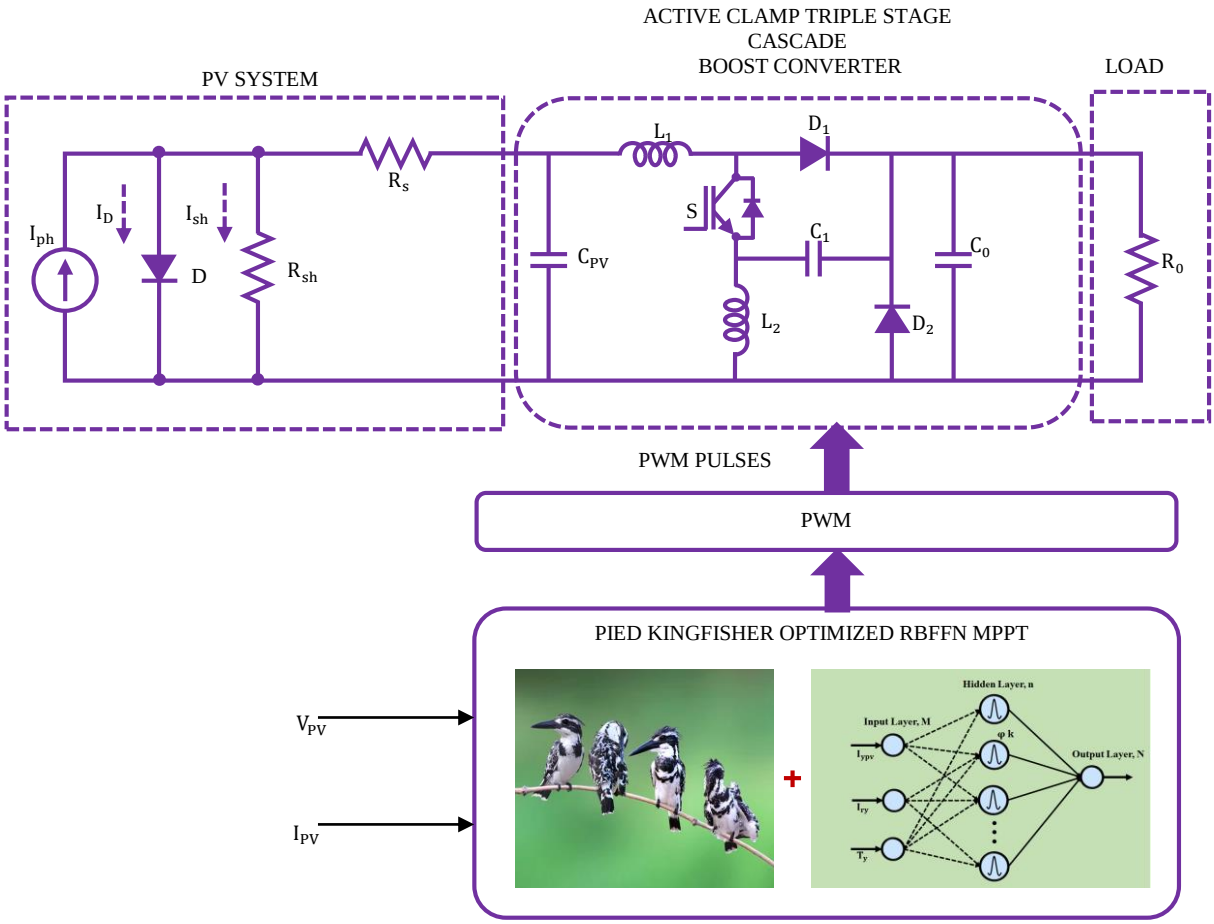

Fig. 1 Block diagram for continuous power generation

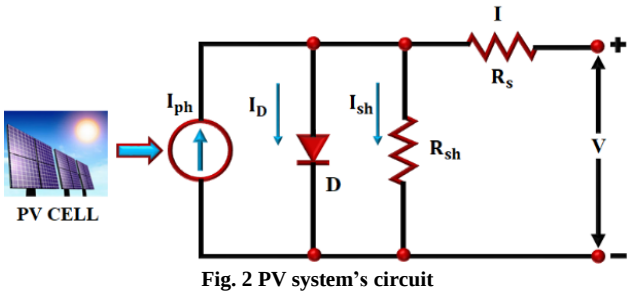

Fig. 2 PV system's circuit

$$I_x - I_D - I_{Rp} = I_{PV} \quad (1)$$

$$I_0 \left[exp\left(\frac{qV_D}{AKT_O}\right) - 1 \right] = I_D \quad (2)$$

$$I_{s0} \left(\frac{T}{T_0}\right)^3 exp\left[\frac{qE_g}{AK}\left(\frac{1}{T_0} - \frac{1}{T}\right)\right] = I_0 \quad (3)$$

$$V_D = V + I_{PV}.R_s \quad (4)$$

$$I_{sc}\frac{S}{S_0} + C_t(T - T_0) = I_x \quad (5)$$

$$I_{Rp} = \frac{V_D}{R_p} \quad (6)$$

$$V_s = N_s.V \quad (7)$$

$$I_p = N_p.I_{PV} \quad (8)$$

Where the cell terminal's voltage is signified by I_{PV} and $V.I_x$ It is a DC current source, and the internal diode current is denoted by I_D, while the shunt resistance current is denoted by$I_{Rp}.I_0$ is the dark saturation current, ideality factor is A, and the electrical charge is denoted by $q\ and$. Internal diode voltage is V_D.

The Boltzmann constant is k, and temperature And irradiance are $T_O$and $S_0$and I_{s0}stands for diode saturation current. The ambient temperature is denoted by T, and the band gap energy is denoted byE_g, series and shunt resistors are R_p. The temperature coefficient is denoted byC_t. The numbers of PV cells in parallel and series arrays are indicated by $N_s$andN_p. Then, the ACTSCB converter is exploited to elevate the PV system's voltage to match the necessities of the load.

4.2. ACTSC Boost Converter

The ACTSC Boost converter is a high-gain step-up design that effectively amplifies voltage by combining an active clamp branch with three cascaded boosting stages, as represented in Figure 3. Compared to traditional high-gain topologies, the ACTSC Boost converter offers high voltage gain while reducing voltage stress on the switch and DC-link ripple.

Even in situations of partial shade, it guarantees effective power extraction without adding further parts or complexity. The ACTSC Boost converter comprises one switch S, 2 diodes. D_1 and D_2, capacitors C_1 and C_2 and2 inductors (L_1 and L_2). The primary switch controls the coordinated charging and discharging cycles of inductors L_1 and L_2,enablingmulti-stage\energy ccumulation and transfer.

In order to facilitate sequential boosting and prevent reverse current during energy transfer between stages, diodes D_1 and D_2 offer directed current flow. The output capacitor C_O filters the final DC high voltage before sending it to the load, while the intermediate capacitor C_1 stores and releases energy to sustain continuous boosting over cascaded sections. Lower losses are ensured by the active clamp network across the switch, which suppresses voltage spikes and absorbs leakage energy. The ACTSC Boost converter offers high gain, minimal component stress, and exceptional efficiency for PV applications. It functioned in 2 operating stages that are discussed below. Figure 4 depicts the waveform of the ACTSC Boost converter.

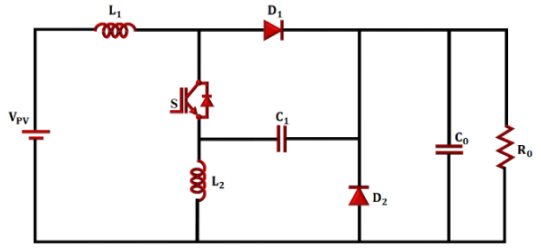

Fig. 3 ACTSC Boost converter's circuit

Stage 1- When S is activated, the current from V_{PV} flows via L_1 causing a current of L_1 to increase and store magnetic energy. Diode D_1 is inactive and C_O supplies the energy to load, as seen in Figure 5(a). By applying KVL,

$$V_{L_1} = V_{PV} \tag{9}$$

$$V_{PV} - V_{C_1} = V_{L_2} \tag{10}$$

$$i_{L_1} = i_{PV} \tag{11}$$

$$i_{L_1} = i_S + i_{C_1} \tag{12}$$

$$i_{C_1} = i_{L_2} + i_{D_2} \tag{13}$$

$$V_O = V_{C_O} \tag{14}$$

$$\frac{diL_1}{dt} = \frac{V_{PV}}{L_1} \tag{15}$$

$$\frac{diL_2}{dt} = \frac{V_{PV} - V_{C_1}}{L_2} \tag{16}$$

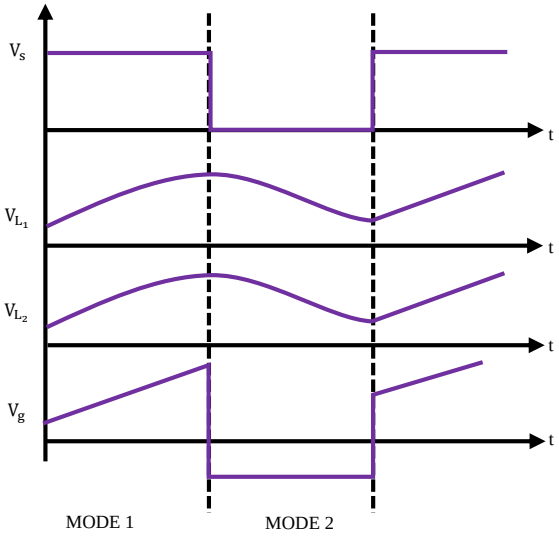

Fig. 4 Waveform of ACTSC boost converter

Stage 2- When S is in the off condition, it causes the energy stored in L_1 is released toward the output via D_1. The inductor L_1 discharges its energy into C_O and the load. Here, D_2 is reverse-biased and L_2 is not conducted, as revealed in Figure 5(b).

$$0 = V_{PV} - V_{L_1} - V_O \quad (17)$$

$$V_{L_2} = V_{C_1} \quad (18)$$

$$i_{L_1} + i_{C_1} = i_{PV} \quad (19)$$

$$i_{D_1} = i_{L_1} \quad (20)$$

$$i_{C_0} + i_{R_0} = i_{D_1} \quad (21)$$

$$i_{C_1} = i_{L_2} \quad (22)$$

$$\frac{diL_1}{dt} = \frac{V_{PV} - V_O}{L_1} \quad (23)$$

$$\frac{diL_2}{dt} = \frac{V_{C_1}}{L_2} \quad (24)$$

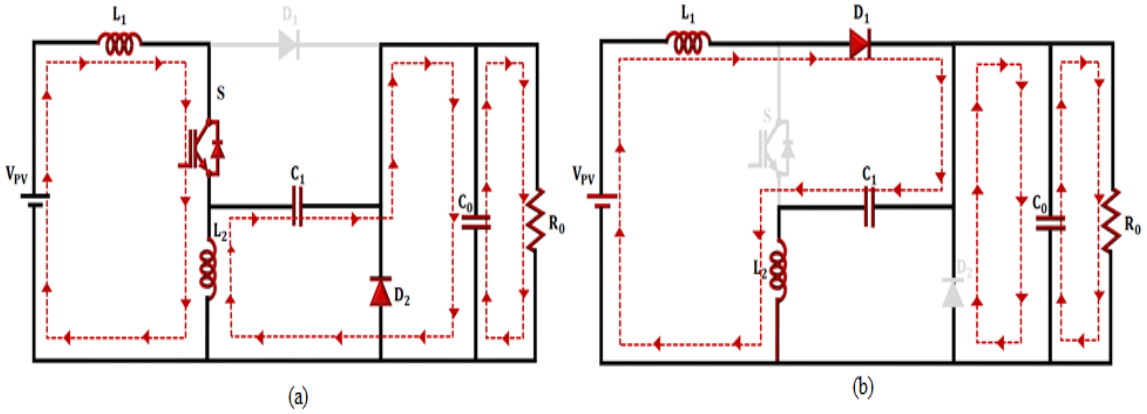

Fig. 5 Stages of ACTSC boost converter (a) Stage 1, and (b) Stage 2.

The voltage gain is,

$$DV_{PV} = (1 - D)(V_{PV} - V_O) = 0 \quad (25)$$

$$V_O = \frac{V_{PV}}{1-D} \quad (26)$$

$$\frac{V_O}{V_{PV}} = \frac{1}{1-D} \quad (27)$$

$$D\left(V_{PV} - V_{C_1}\right) = (1 - D)\left(V_{C_1}\right) = 0 \quad (28)$$

$$V_{PV}D - DV_{C_1} + (1 - D)V_{C_1} = 0 \quad (29)$$

$$V_{PV}D = V_{C_1}(2D - 1) \quad (30)$$

$$V_{C_1} = \frac{D}{2D-1}V_{PV} \quad (31)$$

The voltage stress on S is,

$$V_S = V_{PV} + V_{C_1} \quad (32)$$

Substitute expression (31) in (32),

$$V_S = V_{PV}\left(1 + \frac{D}{2D-1}\right) \quad (33)$$

$$V_{PV}\frac{2D-1+D}{2D-1} = V_{PV}\frac{3D-1}{2D-1} \quad (34)$$

The voltage stress on D_1 *and* D_2 are,

$$V_O = V_{D_1,Stress} \quad (35)$$

$$\frac{V_{PV}}{1-D} = V_{D_1,Stress} \quad (36)$$

$$V_{C_1} = V_{D_2,Stress} \quad (37)$$

$$\frac{D}{2D-1}V_{PV} = V_{D_2,Stress} \quad (38)$$

Where the voltage across C_1, C_2, L_1, L_2, D_1 *and* D_2 are $V_{C_1}, V_{C_2}, V_{L_1}, V_{L_2}, V_{D_1}$ *and* V_{D_2} and the current across L_1, C_O, L_2, C_1 *and* R_O are $i_{L_1}, i_{C_O}, i_{L_2}, i_{C_1}$ *and* i_{R_0}. Despite the benefits of better gain and efficacy of the ACTSC Boost converter, there is an issue with voltage stability. Thus, the PKOA-RBFNN-MPPT controller is employed to enhance further the performance of the system, which efficiently tracks the utmost power of the PV system.

4.3. PKOA-Based RBFNN-MPPT Controller

In PV systems, the RBFNN-MPPT controller constantly extracts the utmost power from solar panels in a variety of environmental situations. In contrast to traditional MPPT techniques, the PKOA algorithm permits quicker convergence to the global Maximum Power Point under dynamic irradiance and temperature fluctuations by optimally tuning the RBFNN weights and spread parameters in real-time. In contrast to conventional techniques, which frequently call for intensive offline training, it lowers steady-state oscillations and enhances tracking accuracy. In order to quickly modify the

operating point and precisely model the nonlinear features of PV modules, it uses an artificial neural network with radial basis functions. As presented in Figure 6, RBFNN is a 3-layer network with input, hidden, and output layers. The activation function is the Gaussian function. The output layer generates a new space by mapping the non-linearity as a linear combiner. For a dataset of n input variables, there are n hidden layers that correspond to each duty cycle value.

$$M^y = \begin{bmatrix} I_{ry} \\ T_y \\ I_{ypv} \end{bmatrix} \tag{39}$$

$$N^y = D^y, y = 1,2,..n. \tag{40}$$

$$\varphi = \begin{pmatrix} \varphi_1^1 & \varphi_2^1 & \varphi_x^1 \\ \varphi_1^2 & \varphi_2^2 & \varphi_x^2 \\ \varphi_1^n & \varphi_2^n & \varphi_x^n \end{pmatrix} \tag{41}$$

Where r is a scalar number r that represents the width of the RBF. The Gaussian function is,

$$\varphi_k(M^y) = \exp\left(\frac{\|M^y - C_k\|^2}{r^2}\right) \tag{42}$$

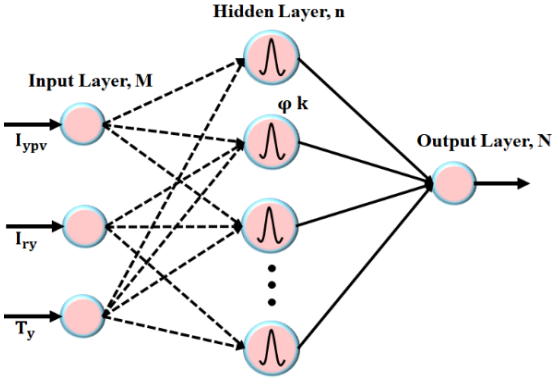

Fig. 6 RBFNN-MPPT controller's structure

The output layer is,

$$N_I^y = \sum_{k=1}^{n} w_{kI}\varphi_k(M^y) + b_k \tag{43}$$

The PKOA is employed to tune the parameters of RBFNN-MPPT, comprising the widths, centers, and output weights. In the initialization phase, each candidate solution in PKOA indicates a set of RBFNN parameters. The position is initialized as,

$$X_{i,j} = LB_j + \left(UB_j - LB_j\right).rand, j = 1,2,\dots,Dim, i = 1,2,\dots,N. \tag{44}$$

Where the upper and lower bounds are UB_j and LB_j, population size is N, and optimized parameters are dim. The PKOA establishes a distinct set of RBFNN parameters that enhances convergence performance in varying conditions. In the exploration phase, the PKOA imitates the kingfisher's aquatic and aerial hunting strategies to explore the multidimensional search space of RBFNN parameters efficiently. When the random value is less than 0.8, this phase is activated, and either the perching or circling approach is selected with equal probability. In the perching strategy, the spatial observation is used to explore new RBFNN parameters.

$$X_i(t) + \left(X_j(t) - X_i(t)\right)\alpha.T = X_i(t+1), j \neq i \tag{45}$$

Where the current and updated parameter sets are denoted by$X_i(t)$ $and X_i(t+1)$. The perturbation factor is indicated as,

$$alpha = 2.rand(1, Dim) - 1 \tag{46}$$

The dynamic adjustment factor governs the exploration step size as,

$$T = \left(e - e^{\left(\frac{t-1}{Max_{iter}}^{1/BF}\right)}.\cos(Crest\_angles)\right) \tag{47}$$

The random angle simulating visual scanning direction as,

$$Crest\_angles = 2\pi.rand \tag{48}$$

The circling strategy focuses on refining the RBFNN parameter tuning around the near-optimal MPP conditions. T factor is refined to emulate rapid hovering and precision adjustment as,

$$T = beating\_rate.\left(\frac{t^{1/BF}}{Max\_iter^{1/BF}}\right) \tag{49}$$

$$beating\_rate = rand.\frac{PKO\_Fitness(j)}{PKO\_Fitness(i)} \tag{50}$$

Where the fitness value of i in the population is denoted as $Fitness\ (i)$ and the fitness value of j in the population is $Fitness\ (j)$, and wing beat frequency is denoted as $beating_{rate}$. This exploration phase allows the PKOA to balance global search and local refinement efficiently, and assures the robust tuning of RBFNN-MPPT parameters. In the exploitation phase, PKOA transitions from broader exploration to precise fine-tuning of RBFNN-MPPT parameters. It is activated when the random control variable exceeds 0.8, enabling the population to focus on predicted better regions in the exploration phase. The update of position is denoted as,

$$X_i(t) + HA.o.\alpha.(b - X_{best}(t)) = X_i(t+1) \tag{51}$$

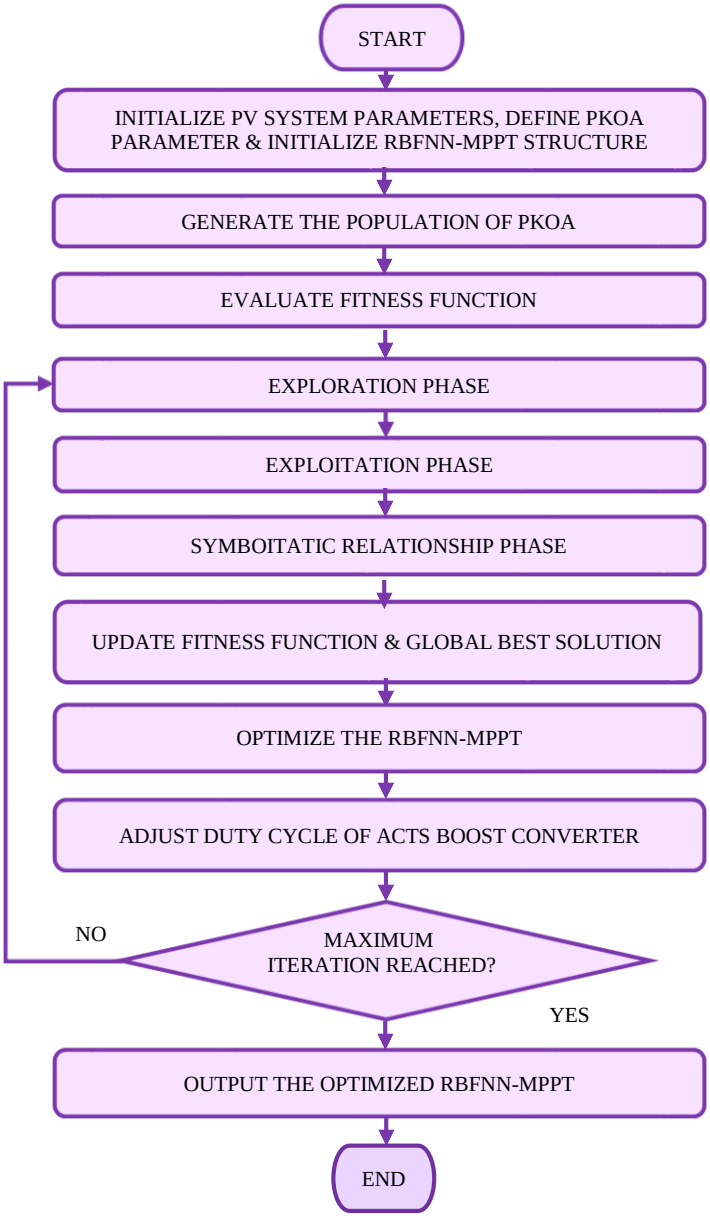

Fig. 7 Flowchart of PKOA-based RBFNN-MPPT controller

Where the best RBFNN-MPPT parameter is denoted as $X_{best}(t)$. The temporary point directs the individual toward the optimal region as,

$$b = X_i(t) + o^2 . rand \, . X_{best} \tag{52}$$

It allows the PKOA to perform controlled local exploitation near the best RBFNN-MPPT parameter set. The hunting ability simulates the adaptive strike strength of the kingfisher and predicts movement intensity based on fitness value as,

$$HA = rand . \frac{PKO\_Fitness(i)}{Best\_Fitness} \tag{53}$$

Here, the best fitness is denoted by $Best\_Fitness$. The time decay factor manages convergence dynamics, assures the quick enhancement in early iterations, and stabilization in later stages as:

$$o = exp\left(-\left(\frac{t}{Max\_iter}\right)^2\right) \tag{54}$$

The PKOA allows focused refinement of RBFNN-MPPT parameters, which assures quicker convergence, reduced oscillations, and improved tracking in fluctuating conditions. In the symbolic phase, the PKOA introduces a cooperative mechanism inspired by the mutualistic interaction among kingfishers and otters. It is developed to aid the PKOA to

escape local optima and maintain diversity in the RBNN-MPPT parameter set. The foraging efficiency is,

$$PE = PE_{max} - (PE_{max} - PE_{min}).\frac{t}{Max\_iter} \quad (55)$$

When a random value exceeds $(1 - PE), t$he symbiotic perturbation is applied to introduce new variations in RBFNN-MPPT parameters.

$$X_m(t) + o.\alpha.|X_i(t) - X_n(t)| = X_i(t+1) \quad (56)$$

Where two arbitrarily selected solutions are represented as X_m and X_n. When the random number is less than $(1 - PE)$, the PKOA retains the current parameter as,

$$X_i(t+1) = X_i(t) \quad (57)$$

It enhances the robustness of the MPPT controller by assuring consistent convergence to the global optima, thereby attaining quicker tracking response in varying environmental conditions. It also attains faster convergence with minimal steady state oscillations and enhanced tracking efficiency.

5. Results and Discussions

This section examines the outcomes of the PKOA-RBFNN-MPPT controller and ACTSC Boost converter for constant power generation and is analyzed with other conventional approaches. The specification of the parameter is revealed in Table 2.

Table 2. Parameter specification

Parameters	Specification
PV system	
Rated Power	5 KW
Panel's peak power	250 W
Voltage (Open Circuit)	37.25V
Peak Current (Maximum)	8.35 A
Current (Short Circuit)	8.95 A
Peak Voltage (Maximum)	29.95 V
N_S	2
N_P	11
ACTSC Boost Converter	
C_1	22 μF
L_1 and L_2	4.7mH
C_O	2200 μF
Switching frequency	10kHz

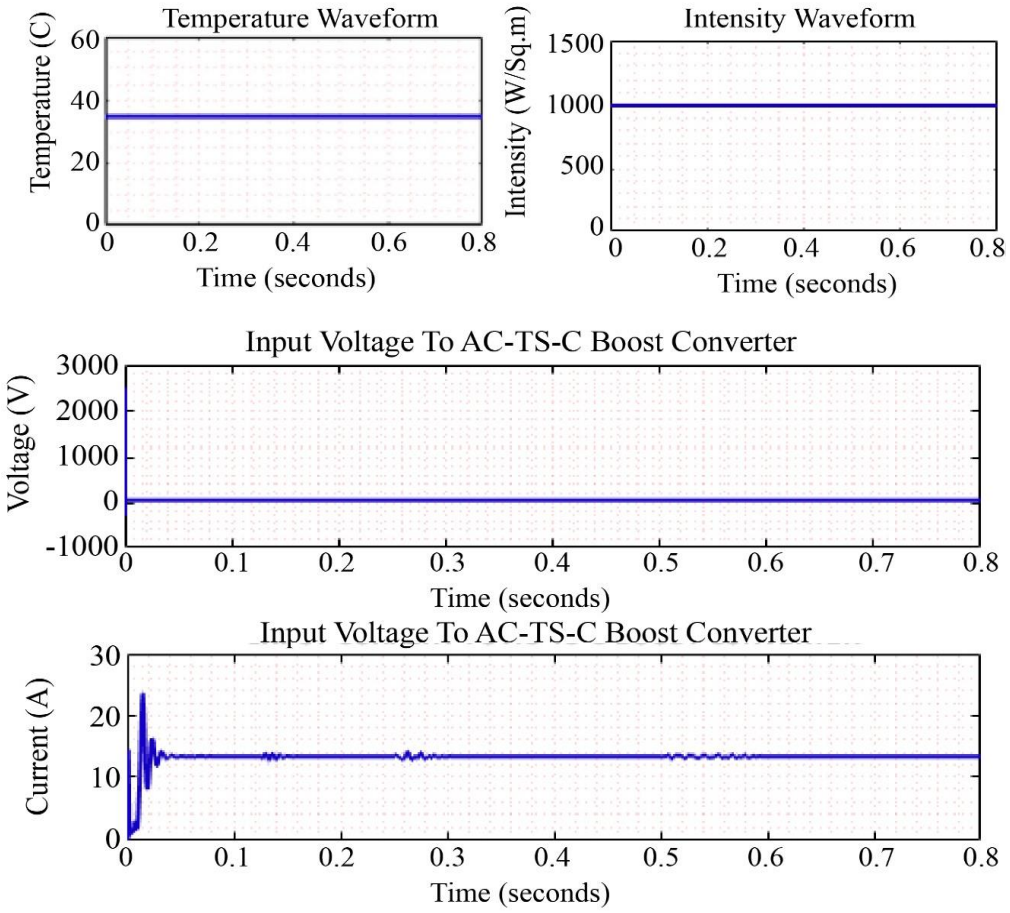

Fig. 8 Waveform of PV system

The PV waveform system under a constant scenario is shown in Figure 8. The temperature and intensity are constantly maintained at 35℃ and 1000 $\left({}^{W}/_{sq.m}\right)$ in the system. Then, the voltage on the input side is persistently sustained at 53 V while the current on the input side is initially fluctuated in the beginning, and after 0.05 s, it is continuously sustained at 13 A, leading to the enhanced efficiency.

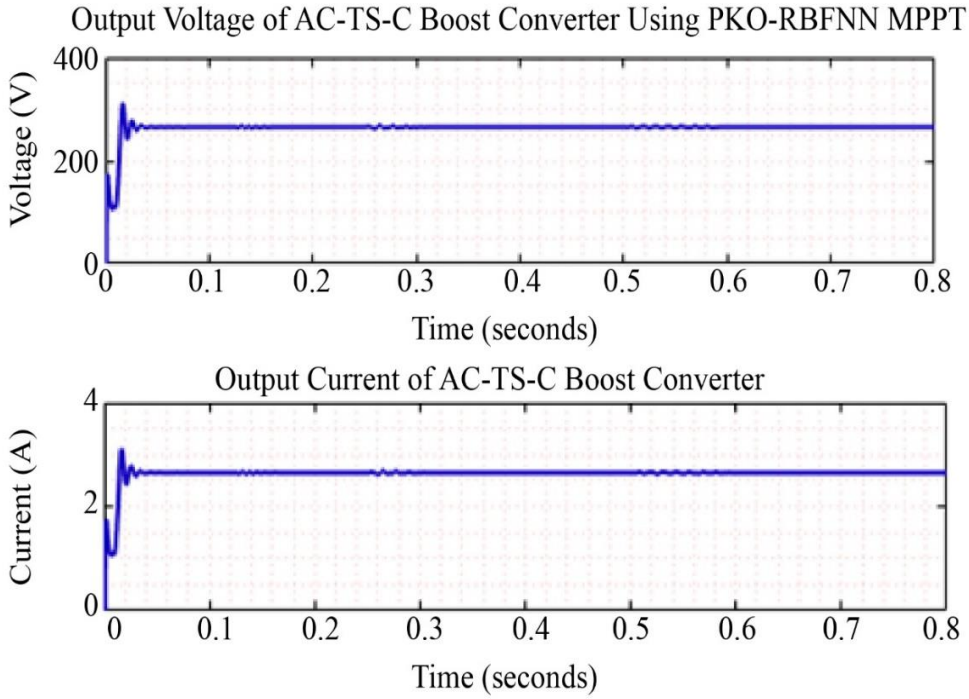

Fig. 9 Output waveform of ACTSCB converter

Figure 9 depicts an output waveform of the ACTSCB converter, in which the output voltage is varied in the early stage due to the absence of an MPPT controller. After 0.05s, it is steadily sustained at 260 V using the PKOA-RBFNN-MPPT controller. Thus, the voltage gain is enhanced at a 52% duty cycle. Also, the output current has random fluctuations in the starting stage and then settles at 2.5 A with the aid of the PKOA-RBFNN-MPPT controller.

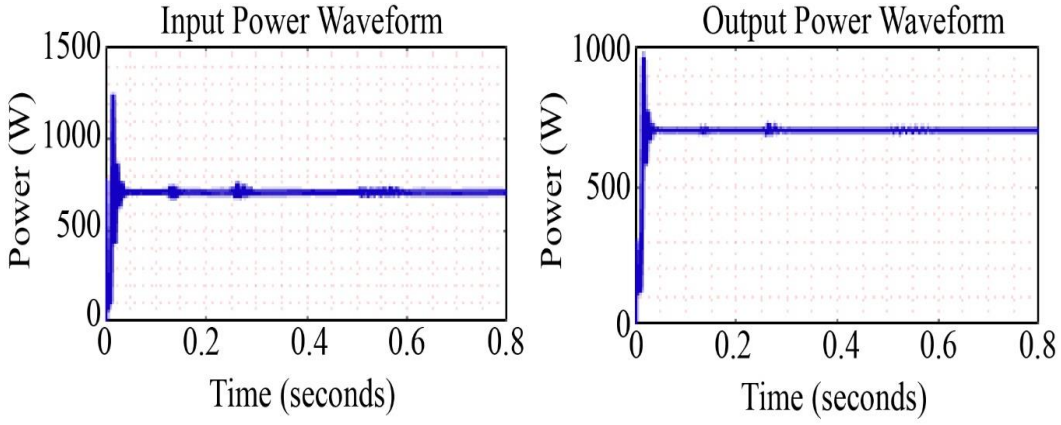

Fig. 10 Power waveform of ACTSCB converter

The power waveform of the ACTSCB converter is represented in Figure 10. The input power is gradually reduced and stabilized at 713.019 W, although the output power is settled at 703.476 W throughout the system. Figure 11 reveals the waveform of the PV system. Here, the temperature and intensity are raised and settled at 35℃ and 1000 $\left({}^{W}/_{sq.m}\right)$ in the complete system. Meanwhile, the input voltage is continued at 53.12 V while the current on the input side is steadily maintained and the input current is constantly settled at 13.32 A. So, the voltage stress is reduced at a 52% -53%

duty cycle, which leads to the converter being exploited in real-time applications. The output responses of the ACTSCB converter are revealed in Figure 12. The voltage and current on the output side are slowly raised and settled at 260 V and 2.5 A in the entire system due to the aid of the PKOA-RBFNN-MPPT controller.

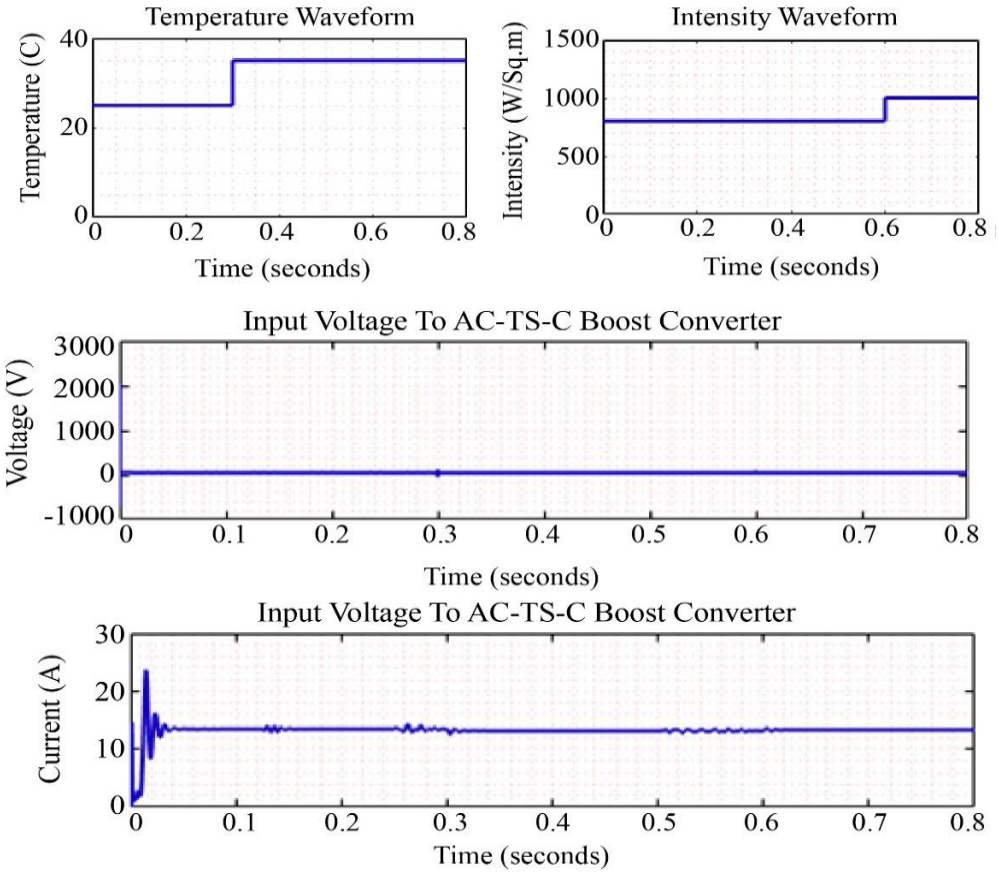

Fig. 11 Responses of the PV system

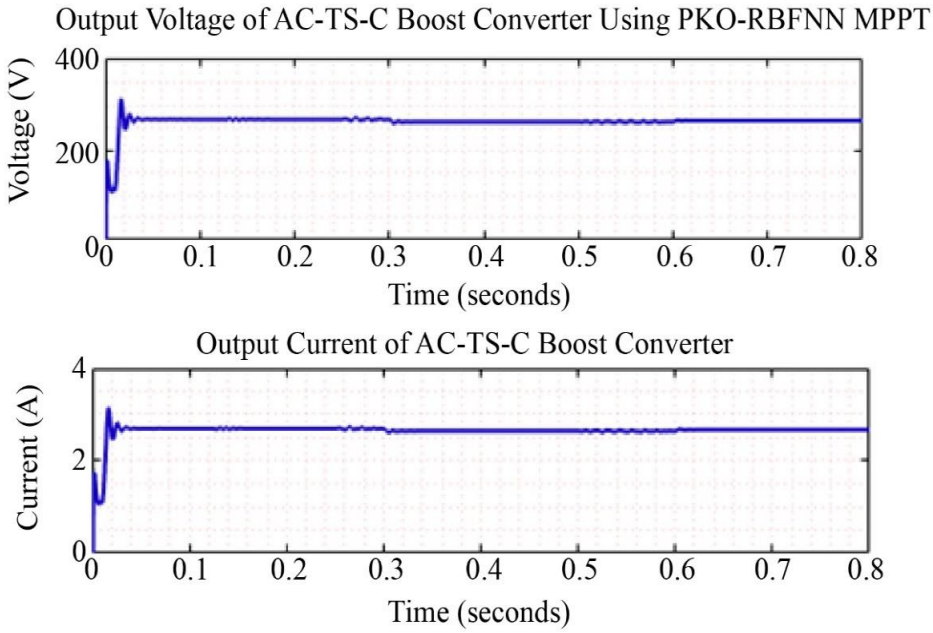

Fig. 12 Output responses of the ACTSCB converter

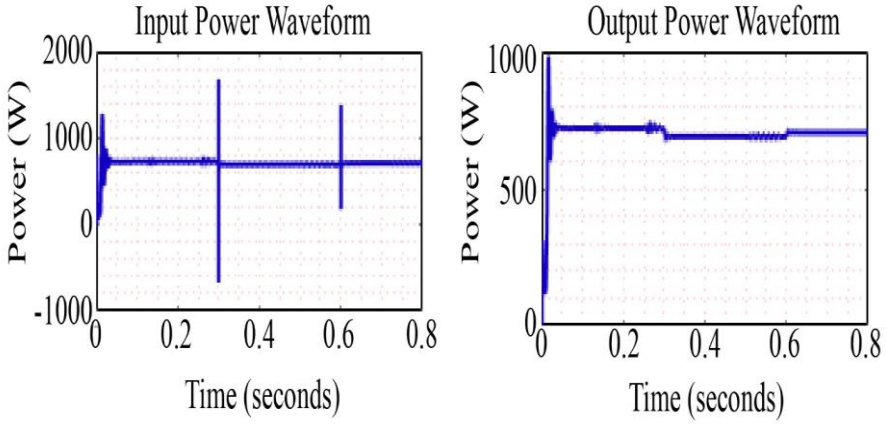

Fig. 13 Power waveform of ACTSCB converter

The power waveform of the ACTSCB converter is represented in Figure 13. The input power is settled at 713.019 W, and the output power is sustained at 703.476 W in the entire system with little oscillations.

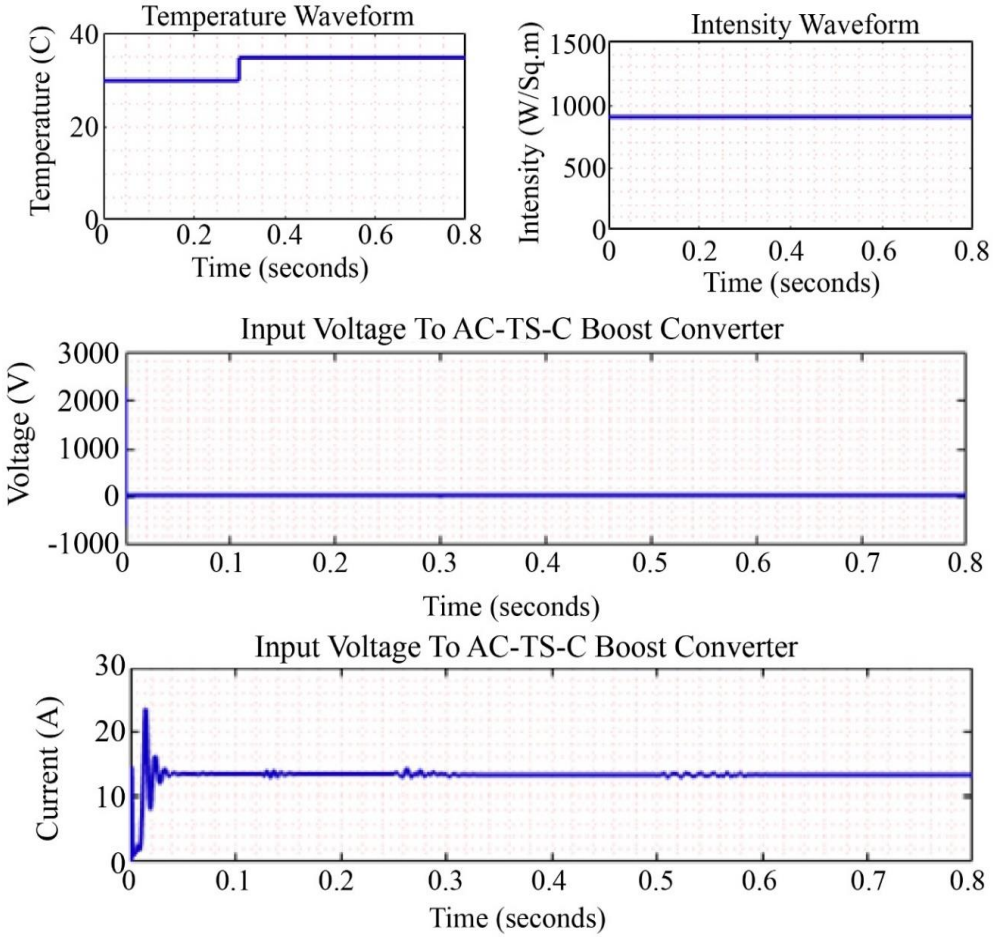

Fig. 14 Waveform of PV system

The waveform of the PV system in varying temperature and constant intensity conditions is revealed in Figure 14. The temperature is varied and settled at 35℃, while the intensity has a constant value of 1000 $\left({}^{W}/_{sq.m}\right)$. Thus, the voltage on the input side is sustained at 53 V, and the input current is sustained at 13 A, which leads to better performance of the converter.

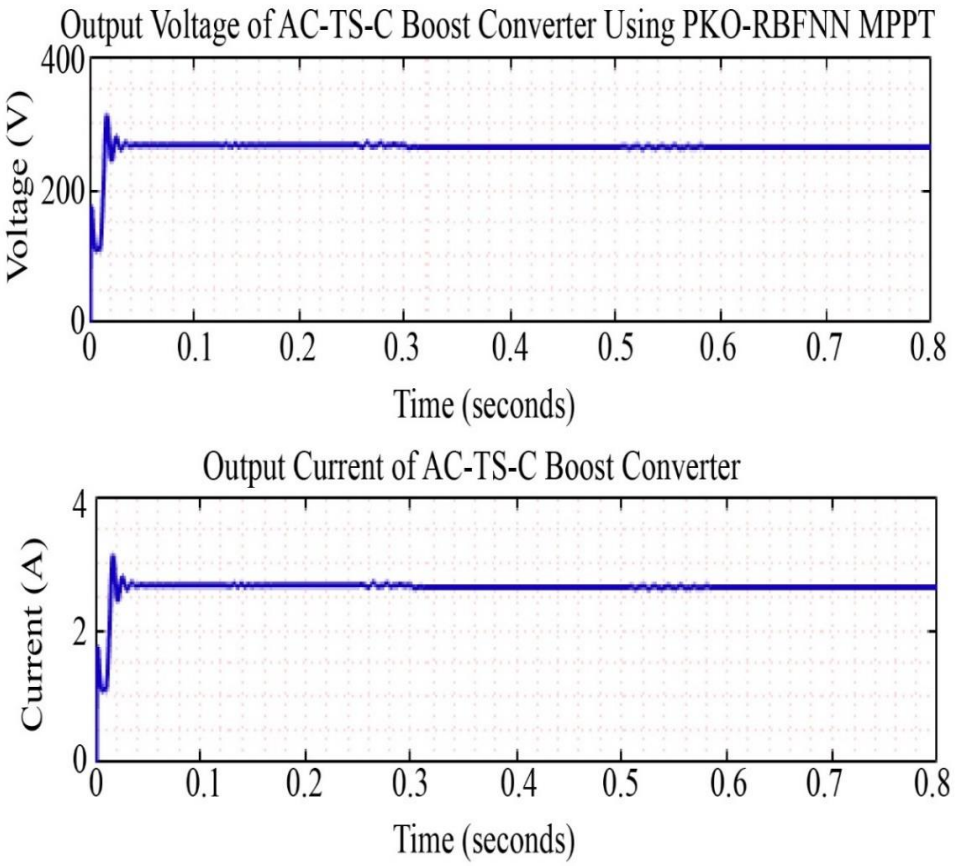

Fig. 15 Output waveform of ACTSCB converter

The ACTSCB converter's output responses are shown in Figure 15. The voltage on the output side is sustained at a constant value of 260 V while the output current is settled at 2.5 A, which offers a better voltage gain. The power waveform of the ACTSCB converter is presented in Figure 16. Here, the input power is initially varied and settles at 713.019 W, while the output power remains at 703.476 W. The responses of the PV system under partial shading are shown in Figure 17.

The temperature is sustained at 35℃, and the intensity is reduced and settled at $1000\ (^{W}/_{sq.m})$. Then, the input voltage and current are maintained at 53 V and 13 A. Figure 18 illustrates the output responses of the ACTSCB converter. The efficacy of the ACTSC Boost converter is enhanced due to the constant voltage and current of 260V and 2.5A with the presence of the PKOA-RBFNN-MPPT controller.

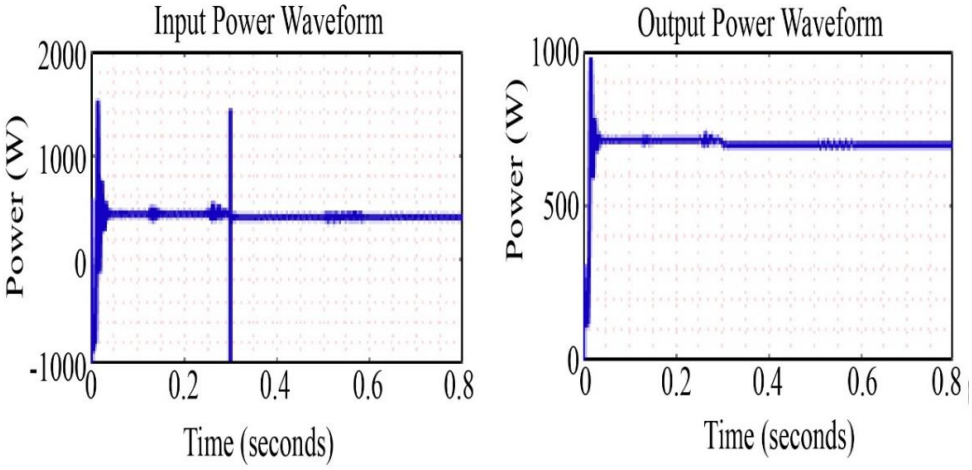

Fig. 16 Power waveform of ACTSCB converter

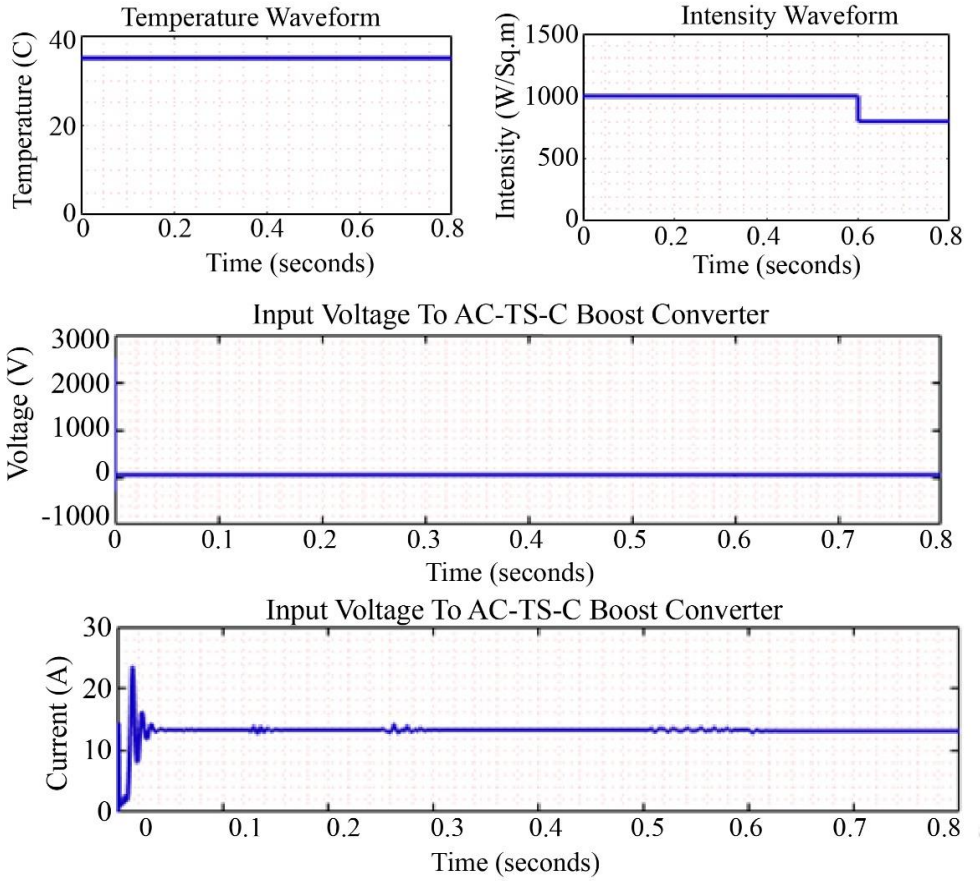

Fig. 17 Waveform of PV system

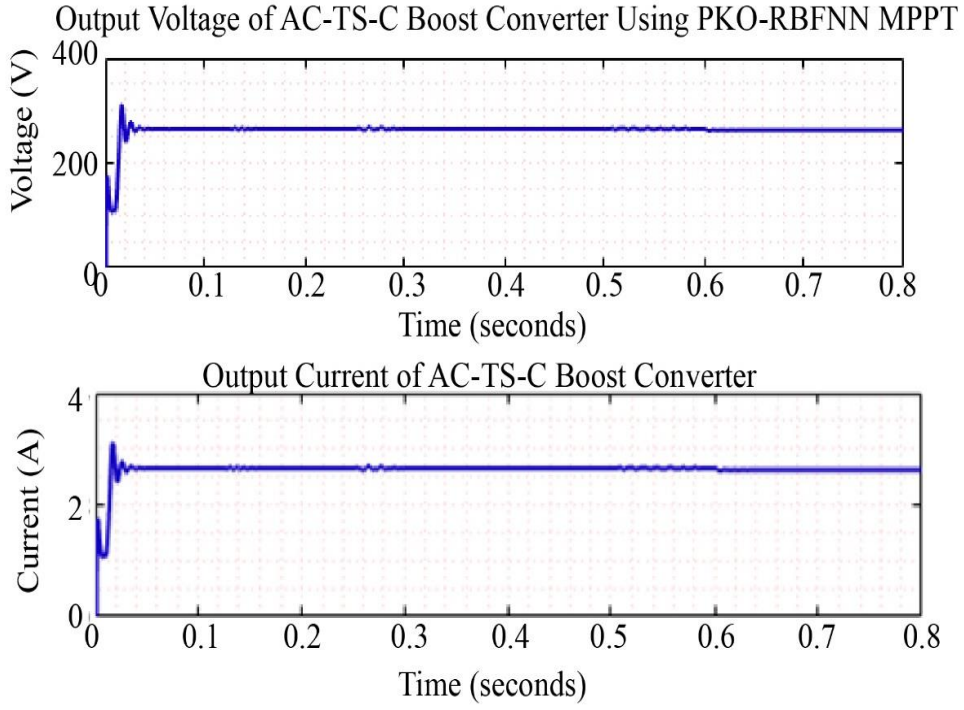

Fig. 18 Output waveform of ACTSCB converter

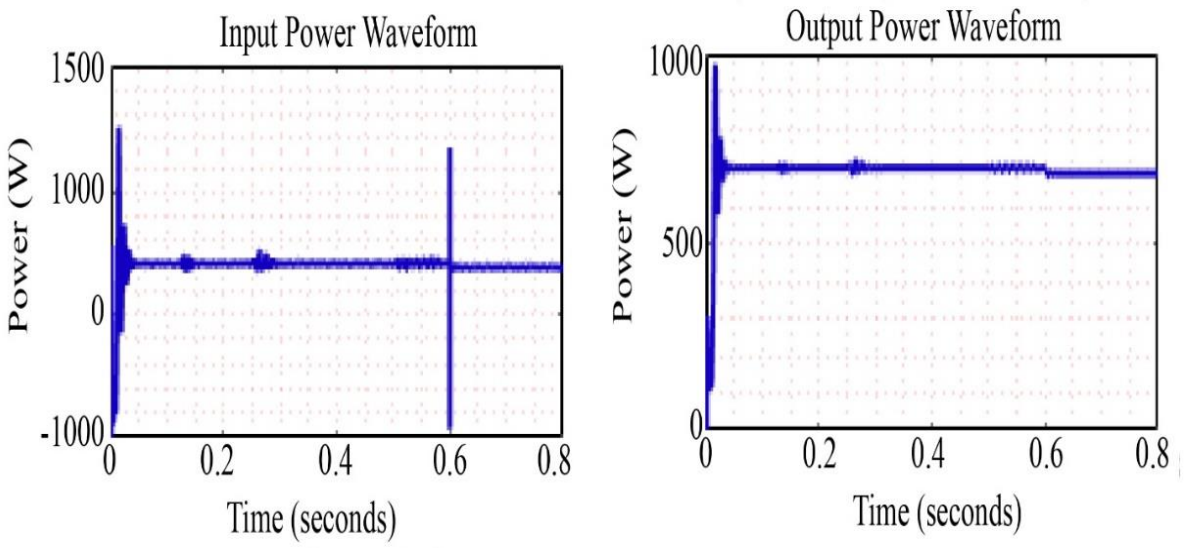

Fig. 19 Power waveform of ACTSCB Converter

The power waveform of the ACTSCB converter is shown in Figure 19, where the input power is sustained at 713.019 W and the output power is settled at 703.476W, providing better reliability in real-time applications.

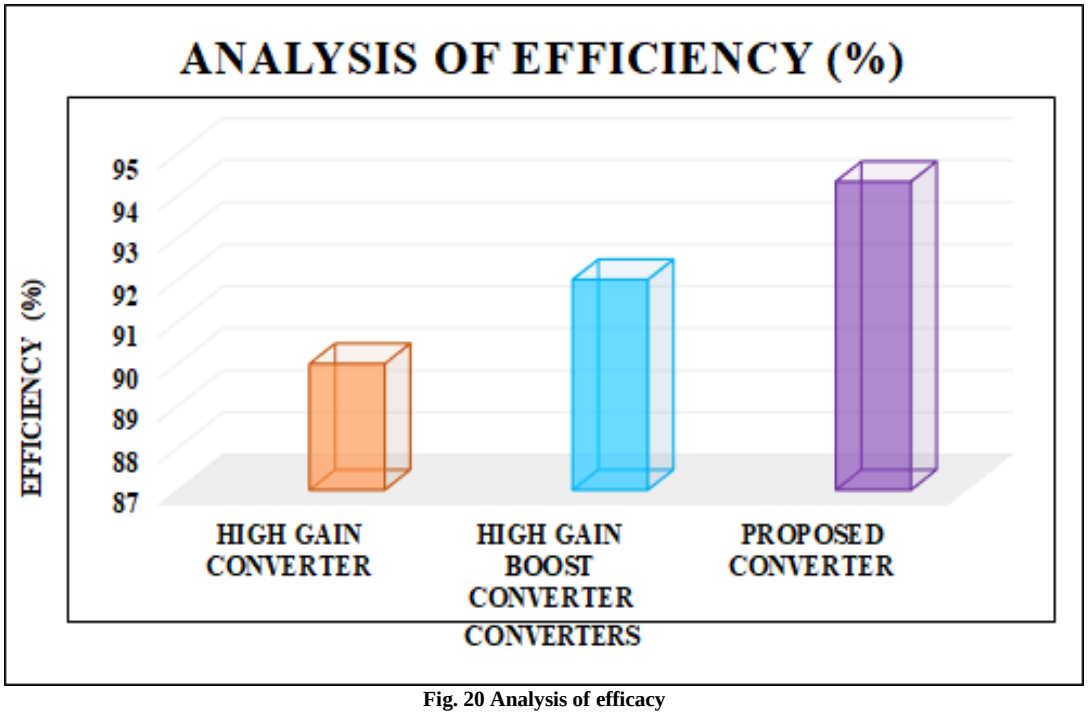

Fig. 20 Analysis of efficacy

Figure 20 depicts the analysis of the efficacy of the High Gain Boost Converter [28], which achieved an efficiency of 92%, and the High Gain Converter [29], which demonstrated an efficiency of 90%. Among others, the ACTSC Boost converter has the highest efficiency of 94.33%, demonstrating it is well-suited for real-world applications. The analysis of the voltage gain of the Switched Inductor/Capacitor Converter [30], High Step-Up Converter [31], Switched Inductor Step-Up Converter [32], Interleaved Converter [33], and the ACTSC Boost converter is presented in Figure 21. The Switched Inductor/Capacitor Converter provides the lowest voltage gain, while the ACTSC Boost converter obtains the largest gain, closely followed by the Interleaved Converter and High Step-Up Converter. It increases power conversion efficiency by ensuring a higher output voltage at lower duty cycles. For high-step-up PV applications requiring greater voltage enhancement and efficiency, the ACTSC Boost converter is beneficial.

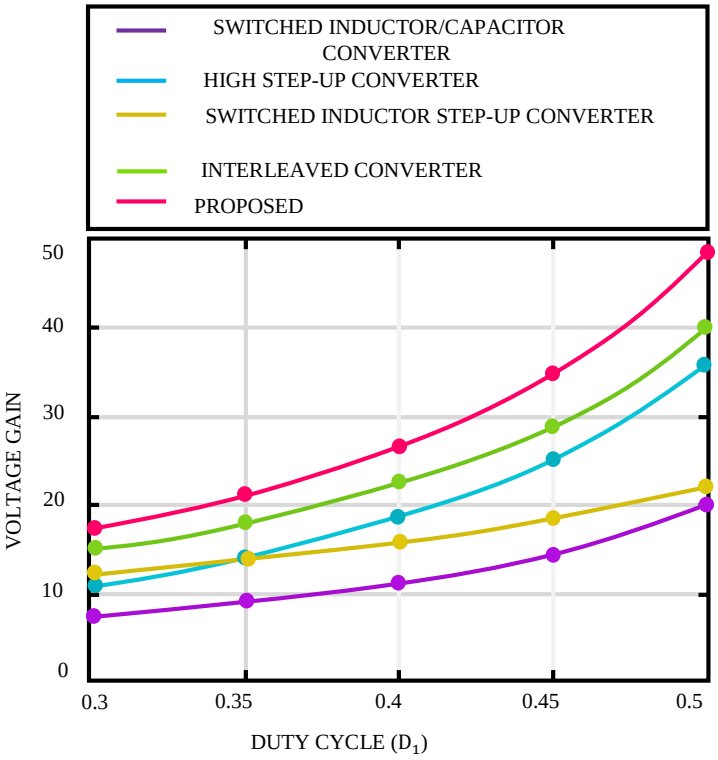

Fig. 21 Analysis of Voltage Gain

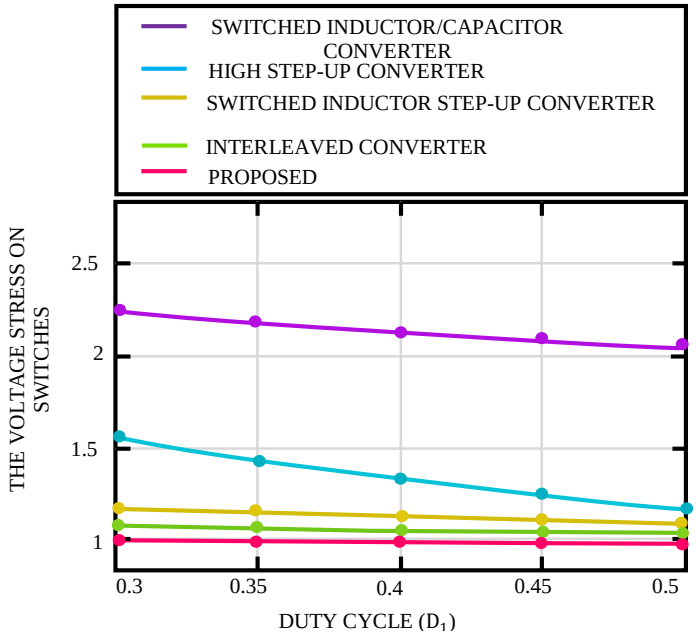

Fig. 22 Analysis of Voltage Stress

Figure 22 shows the analysis of switch voltage stress for the Switched Inductor/Capacitor Converter [30], High Step-Up Converter [31], Switched Inductor Step-Up Converter [32], Interleaved Converter [33], and the ACTSC Boost converter. The ACTSC Boost converter has the lowest voltage stress, reducing switching losses and improving reliability. On the other hand, the Switched Inductor/Capacitor Converter is less effective for high-power applications due to its maximum voltage stress. The Switched Inductor Step-Up Converter and Interleaved Converter exhibit moderate stress levels. The ACTSC Boost converter is perfect for effective PV systems because it reduces voltage stress, which improves thermal management and extends component lifespan.

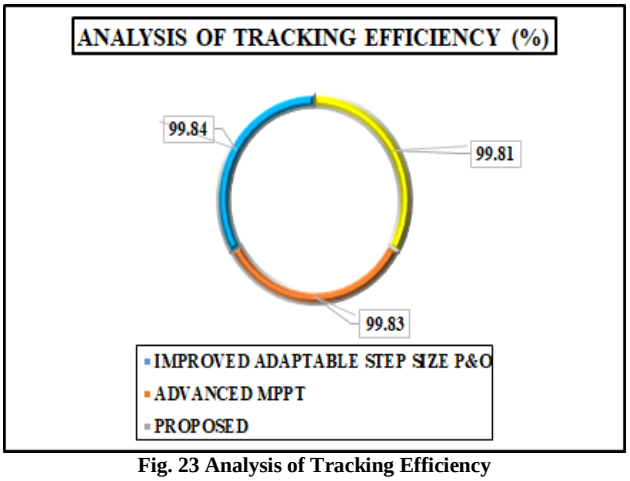

Fig. 23 Analysis of Tracking Efficiency

Figure 23 compares the tracking efficiency of improved Adaptable Step Size P&O [34], Advanced MPPT [11], and the Proposed MPPT algorithm. With an efficiency of 99.81%, the Improved Adaptable Step Size P&O approach is the most effective, followed closely by the Advanced MPPT method with 99.83%.

The highest efficiency of the proposed approach is 99.84%, indicating enhanced performance. The analysis of the converter in terms of component counts and voltage gain is displayed in Table 3. The proposed converter has the least component count among others, indicating a reliable and compact design.

Table 3. Analysis of converters

Converters	Number of components	Voltage gain
Switched Inductor/Capacitor Converter [30]	16	$\frac{1+3D_1-D_2}{1-D_1-D_2}$
Non-isolated Converter [35]	10	$\frac{2N+1-ND}{1-D}$
Switched-Inductor-High Step-Up Converter [36]	12	$\frac{(3N-1)D+N-1}{(1-D)(N-1)}$
Non-isolated Dual-output single-input converter [37]	14	$\frac{2}{1-D}$
High-gain boost converter [38]	8	$\frac{1+D}{1-D}$
Proposed	7	$\frac{1}{(1-D)}$

6. Conclusion

This research proposes an ACTSC Boost converter with a PKOA RBFNN-MPPT controller for achieving constant power generation by reducing tracking time and steady-state oscillations. The ACTSC Boost converter effectively increases the output voltage while reducing switching losses, ensuring high conversion efficiency and lower switch stress. By intelligently adjusting solar conditions, the RBFNN-MPPT controller, which is optimized by the PKOA, achieves quicker tracking response and less steady-state oscillations around the MPP. By offering an excellent exploration-exploitation balance, PKOA improves the neural network's learning capacity and produces precise and reliable power extraction under varying irradiance levels. The system attains a high efficiency of 94.33% and constant power output appropriate for constant power generation, according to simulation outcomes in MATLAB/SIMULINK tool. It is a viable option for high-performance and sustainable solar energy systems since it guarantees dependable, effective, and intelligent power management.

References

[1] G. Geethamahalakshmi, N. Kalaiarasi, and D. Nageswari, "Fuzzy based MPPT and Solar Power Forecasting using Artificial Intelligence," *Intelligent Automation & Soft Computing*, vol. 32, no. 3, pp. 1667-1685, 2022. [CrossRef] [Google Scholar] [Publisher Link]

[2] K.S. Kavin, and P. Subha Karuvelam, "PV-based Grid Interactive PMBLDC Electric Vehicle with High Gain Interleaved DC-DC SEPIC Converter," *IETE Journal of Research*, vol. 69, no. 7, pp. 4791-4805, 2023. [CrossRef] [Google Scholar] [Publisher Link]

[3] K. Ancy et al., "Antibacterial Activities and Photocatalyzed Degradation of Textile Dyeing Waste Water by Mn and F co-doped TiO_2 Nanoparticles," *Advances in Natural Sciences: Nanoscience and Nanotechnology*, vol. 13, no. 4, pp. 1-12, 2022. [CrossRef] [Google Scholar] [Publisher Link]

[4] M.S. Anandha Prabhu "Biogenic Synthesis of Silver, Gold, and Palladium Nanoparticles using Moringa Oleifera Seeds: Exploring Photocatalytic, Catalytic, and Antimicrobial Activities," *Advances in Natural Sciences: Nanoscience and Nanotechnology*, vol. 15, no. 1, pp. 1-9, 2024. [CrossRef] [Google Scholar] [Publisher Link]

[5] Mostafa Ahmed et al., "Model-based Maximum Power Point Tracking Algorithm with Constant Power Generation Capability and Fast DC-Link Dynamics for Two-Stage PV Systems," *IEEE Access*, vol. 10, pp. 48551-48568, 2022. [CrossRef] [Google Scholar] [Publisher Link]

[6] K.S. Kavin et al., "Improved BRBFNN-based MPPT Algorithm for Coupled Inductor KSK Converter for Sustainable PV System Applications," *Electrical Engineering*, vol. 107, no. 6, pp. 7831-7853, 2025. [CrossRef] [Google Scholar] [Publisher Link]

[7] Alagar Karthick et al., "Deep Learning based State of Charge Prediction for EV Battery Packs," *2025 11th International Conference on Electrical Energy Systems (ICEES)*, Chennai, India, pp. 666-669, 2025. [CrossRef] [Google Scholar] [Publisher Link]

[8] Mahmoud N. Ali et al., "An Efficient Fuzzy-Logic based Variable-Step Incremental Conductance MPPT Method for Grid-Connected PV Systems," *IEEE Access*, vol. 9, pp. 26420-26430, 2021. [CrossRef] [Google Scholar] [Publisher Link]

[9] P. Bhanu et al., "Optimizing Electric Vehicle Charging Station Performance: Integrating Gazelle Optimization Algorithm and Hamiltonian Deep Neural Networks for Reduced Costs and Enhanced Efficiency," *Journal of Energy Storage*, vol. 136, 2025. [CrossRef] [Google Scholar] [Publisher Link]

[10] A.S. Veerendra et al., "Design and Implementation of Active Clamp Flyback Converter for High-Power Applications," *Processes*, vol. 11, no. 10, pp. 1-18, 2023. [CrossRef] [Google Scholar] [Publisher Link]

[11] Abdelkhalek Chellakhi et al., "An Efficient Implementation of Three-Level Boost Converter with Capacitor Voltage Balancing for an Advanced MPPT Approach in PV Systems," *E-Prime-Advances in Electrical Engineering, Electronics and Energy*, vol. 9, pp. 1-26, 2024. [CrossRef] [Google Scholar] [Publisher Link]

[12] Nafis Subhani et al., "An Improved Non-Isolated Quadratic DC-DC Boost Converter with Ultra High Gain Ability," *IEEE Access*, vol. 11, pp. 11350-11363, 2023. [CrossRef] [Google Scholar] [Publisher Link]

[13] Rashid Ahmed Khan et al., "A Novel High-Voltage Gain Step-Up DC-DC Converter with Maximum Power Point Tracker for Solar Photovoltaic Systems," *Processes*, vol. 11, no. 4, pp. 1-23, 2023. [CrossRef] [Google Scholar] [Publisher Link]

[14] Seyed Majid Hashemzadeh et al., "Design and Analysis of a New Coupled Inductor-based Interleaved High Step-Up DC-DC Converter for Renewable Energy Applications," *International Transactions on Electrical Energy Systems*, vol. 2022, no. 1, pp. 1-14, 2022. [CrossRef] [Google Scholar] [Publisher Link]

[15] Maryam Shaabani et al., "A Hybrid Switched-Inductor/Switched-Capacitor DC-DC Converter with High Voltage Gain using a Single Switch for Photovoltaic Application," *Energies*, vol. 16, no. 14, pp. 1-20, 2023. [CrossRef] [Google Scholar] [Publisher Link]

[16] Moussa Sedraoui et al., "Development of a Fixed-Order Controller for a Robust P&O-MPPT Strategy to Control Poly-Crystalline Solar PV Energy Systems," *Scientific Reports*, vol. 15, no. 1, pp. 1-23, 2025. [CrossRef] [Google Scholar] [Publisher Link]

[17] S. Sheik Mohammed, D. Devaraj, and T.P. Imthias Ahamed, "GA-Optimized Fuzzy-based MPPT Technique for Abruptly Varying Environmental Conditions," *Journal of The Institution of Engineers (India): Series B*, vol. 102, no. 3, pp. 497-508, 2021. [CrossRef] [Google Scholar] [Publisher Link]

[18] Ambe Harrison, Njimboh Henry Alombah, and Jean de Dieu Nguimfack Ndongmo, "A New Hybrid MPPT based on Incremental Conductance-Integral Backstepping Controller Applied to a PV System under Fast-Changing Operating Conditions," *International Journal of Photoenergy*, vol. 2023, no. 1, pp. 1-17, 2023. [CrossRef] [Google Scholar] [Publisher Link]

[19] Nagwa F. Ibrahim et al., "Operation of Grid-Connected PV System with ANN-based MPPT and an Optimized LCL Filter using GRG Algorithm for Enhanced Power Quality," *IEEE Access*, vol. 11, pp. 106859-106876, 2023. [CrossRef] [Google Scholar] [Publisher Link]

[20] Kifayat Ullah et al., "Fuzzy-based Maximum Power Point Tracking (MPPT) Control System for Photovoltaic Power Generation System," *Results in Engineering*, vol. 20, pp. 1-10, 2023. [CrossRef] [Google Scholar] [Publisher Link]

[21] S.R. Revathy et al., "Design and Analysis of ANFIS-based MPPT Method for Solar Photovoltaic Applications," *International Journal of Photoenergy*, vol. 2022, no. 1, pp. 1-9, 2022. [CrossRef] [Google Scholar] [Publisher Link]

[22] Ali M. Eltamaly, "A Novel Musical Chairs Algorithm Applied for MPPT of PV Systems," *Renewable and Sustainable Energy Reviews*, vol. 146, pp. 1-19, 2021. [CrossRef] [Google Scholar] [Publisher Link]

[23] Muhannad J. Alshareef, "An Effective Falcon Optimization Algorithm based MPPT under Partial Shaded Photovoltaic Systems," *IEEE Access*, vol. 10, pp. 131345-131360, 2022. [CrossRef] [Google Scholar] [Publisher Link]

[24] Mohammed Taha Kaaitan et al., "A Novel Global MPPT Method based on Sooty Tern Optimization for Photovoltaic Systems under Complex Partial Shading," *Scientific Reports*, vol. 15, no. 1, pp. 1-12, 2025. [CrossRef] [Google Scholar] [Publisher Link]

[25] Chunliang Mai et al., "A Novel MPPT Technology based on Dung Beetle Optimization Algorithm for PV Systems under Complex Partial Shade Conditions," *Scientific Reports*, vol. 14, no. 1, pp. 1-23, 2024. [CrossRef] [Google Scholar] [Publisher Link]

[26] Abdulbari Talib Naser et al., "A Fast-Tracking MPPT-based Modified Coot Optimization Algorithm for PV Systems under Partial Shading Conditions," *Ain Shams Engineering Journal*, vol. 15, no. 10, pp. 1-15, 2024. [CrossRef] [Google Scholar] [Publisher Link]

[27] Chundi Jiang, "African Vulture Optimized RNN Algorithm Maximum Power Point Tracking (MPPT) Controller for Photovoltaic (PV) System," *Measurement: Sensors*, vol. 36, pp. 1-9, 2024. [CrossRef] [Google Scholar] [Publisher Link]

[28] Héctor Hidalgo et al., "A High-Voltage-Gain DC-DC Boost Converter with Zero-Ripple Input Current for Renewable Applications," *Energies*, vol. 16, no. 13, pp. 1-23, 2023. [CrossRef] [Google Scholar] [Publisher Link]

[29] Ramachandran Rajesh, and Natarajan Prabaharan, "Design of New Nonisolated High Gain Converter for Higher Power Density," *International Transactions on Electrical Energy Systems*, vol. 2023, no. 1, pp. 1-10, 2023. [CrossRef] [Google Scholar] [Publisher Link]

[30] Behdad Faridpak et al., "Improved Hybrid Switched Inductor/Switched Capacitor DC-DC Converters," *IEEE Transactions on Power Electronics*, vol. 36, no. 3, pp. 3053-3062, 2020. [CrossRef] [Google Scholar] [Publisher Link]

[31] Vafa Marzang et al., "A High Step-Up DC-DC Converter based on ASL and VMC for Renewable Energy Applications," *Energy Reports*, vol. 8, pp. 12699-12711, 2022. [CrossRef] [Google Scholar] [Publisher Link]

[32] Bekkam Krishna, and V. Karthikeyan, "Active Switched-Inductor Network Step Up DC-DC Converter with Wide Range of Voltage-Gain at the Lower Range of Duty Cycles," *IEEE Journal of Emerging and Selected Topics in Industrial Electronics*, vol. 2, no. 4, pp. 431-441, 2021. [CrossRef] [Google Scholar] [Publisher Link]

[33] Farhan Mumtaz et al., "A Novel Non-Isolated High-Gain Non-Inverting Interleaved DC-DC Converter," *Micromachines*, vol. 14, no. 3, pp. 1-17, 2023. [CrossRef] [Google Scholar] [Publisher Link]

[34] Abdelkhalek Chellakhi, Said El Beid, and Younes Abouelmahjoub, "An Improved Adaptable Step-Size P&O MPPT Approach for Standalone Photovoltaic Systems with Battery Station," *Simulation Modelling Practice and Theory*, vol. 121, 2022. [CrossRef] [Google Scholar] [Publisher Link]

[35] Nasser Yousefi et al., "A Non-Isolated DC-DC Topology with High Voltage Rate based on Magnetic Coupling and Voltage Multiplier Method," *International Journal of Circuit Theory and Applications*, vol. 52, no. 1, pp. 188-206, 2024. [CrossRef] [Google Scholar] [Publisher Link]

[36] Arash Imanlou et al., "A New High Voltage Gain Active Switched-Inductor based High Step-Up DC-DC Converter with Coupled-Inductor," *IEEE Access*, vol. 11, pp. 56749-56765, 2023. [CrossRef] [Google Scholar] [Publisher Link]

[37] Hamid Radmanesh et al., "A Dual-Output Single-Input Non-Isolated DC-DC Converter with Reduced Semiconductors Stress," *International Journal of Circuit Theory and Applications*, vol. 51, no. 2, pp. 594-610, 2023. [CrossRef] [Google Scholar] [Publisher Link]

[38] Ali Faisal Murtaza et al., "Design and Analysis of Series LC Network based High Gain Boost Converter," *Energy Reports*, vol. 13, pp. 3700-3711, 2025. [CrossRef] [Google Scholar] [Publisher Link]